TOOLS

Genome-edited human stem cells expressing fluorescently labeled endocytic markers allow quantitative analysis of clathrin-mediated endocytosis during differentiation

Daphné Dambournet[1], Kem A. Sochacki[2], Aaron T. Cheng[3], Matthew Akamatsu[1] [iD], Justin W. Taraska[2] [iD], Dirk Hockemeyer[1] [iD], and David G. Drubin[1] [iD]

We developed a general approach for investigation of how cellular processes become adapted for specific cell types during differentiation. Previous studies reported substantial differences in the morphology and dynamics of clathrin-mediated endocytosis (CME) sites. However, associating specific CME properties with distinct differentiated cell types and determining how these properties are developmentally specified during differentiation have been elusive. Using genome-edited human embryonic stem cells, and isogenic fibroblasts and neuronal progenitor cells derived from them, we established by live-cell imaging and platinum replica transmission electron microscopy that CME site dynamics and ultrastructure on the plasma membrane are precisely reprogrammed during differentiation. Expression levels for the endocytic adaptor protein AP2μ2 were found to underlie dramatic changes in CME dynamics and structure. Additionally, CME dependency on actin assembly and phosphoinositide-3 kinase activity are distinct for each cell type. Collectively, our results demonstrate that key CME properties are reprogrammed during differentiation at least in part through AP2μ2 expression regulation.

Introduction

The human body consists of hundreds of different isogenic cells in diverse differentiated states, each adapted to carry out a specific function. Previous studies focused largely on gene expression changes that underlie differentiation (Gifford et al., 2013) and govern cell specification (Kreitzer et al., 2013). Here, using clathrin-mediated endocytosis (CME) as a model, we developed a system to study how cell structures and processes are modified for the specific needs of different cell types during differentiation. CME leads to the internalization of receptor–ligand complexes and nutrients through a multistep pathway involving sequential recruitment of proteins that each perform a different function. At a late stage, the GTPase dynamin is recruited to the neck of the clathrin-coated pit (CCP), where it mediates clathrin-coated vesicle (CCV) scission from the plasma membrane (PM; McMahon and Boucrot, 2011; Robinson, 2015). Over the last decade, growing evidence suggested that the timing of endocytic protein recruitment to the PM, as well as the morphology of clathrin-coated structures (CCSs), vary from one cell type to another (Fujimoto et al., 2000; Saffarian et al., 2009; Doyon et al., 2011; Taylor et al., 2011; Grove et al., 2014). However, cell line variability caused

by cancer mutations and genomic instability, and the practice of overexpressing fluorescent fusion proteins, made it unclear whether differences in CME properties reflected programmed changes that support the new function of the differentiated cell, or reflected a nonphysiological phenotype caused by cell pathology (Drubin and Hyman, 2017). Here we developed an isogenic cell system to address such questions and gained new insights into programmed changes that adapt CME for the specific needs of different cell types.

Results

Endocytic site dynamics and morphology change upon stem cell differentiation

Previously, studies of the dynamics and morphology of CME sites were confounded by the fact that different studies used cultured cells derived from different species and tissues, complicating understanding of sources of variation. Additionally, these studies used tissue culture cells derived from cancers, and they used overexpressed fluorescent fusion proteins to investigate protein

[1]Department of Molecular and Cell Biology, University of California, Berkeley, Berkeley, CA;   [2]National Heart, Lung, and Blood Institute, National Institutes of Health, Bethesda, MD;   [3]GlaxoSmithKline, Collegeville, PA.

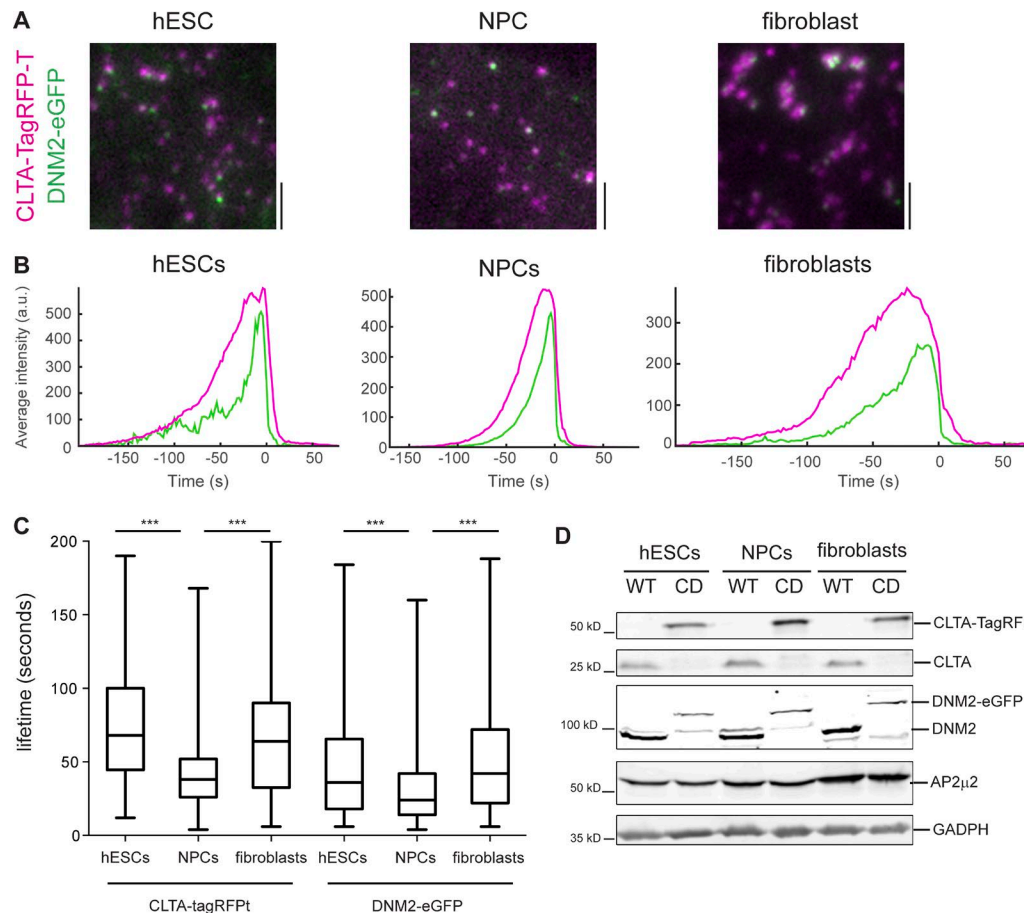Correspondence to David G. Drubin: drubin@berkeley.edu.

Figure 1. **Endocytic dynamics in three isogenic cell types. (A)** TIRFM images of genome-edited, isogenic hESC, NPC, and fibroblast expressing CLTA-TagRFP-T and DNM2-EGFP. Bars, 2 µm. **(B)** Mean fluorescence intensity profile for CLTA-TagRFP-T (magenta line) and DNM2-EGFP (green line) in the three cell types (three to five independent experiments, three to four cells analyzed per experiment, total numbers of tracks represented: hESCs, *n* = 240; NPCs, *n* = 758; fibroblasts, *n* = 164). **(C)** Lifetimes of clathrin and dynamin in the indicated cell types. Box plots show median extended from the 25th to 75th percentiles, minimum and maximum data points (three to five independent experiments, three to four cells analyzed per experiment, total numbers of tracks represented: hESCs, *n* = 240; NPCs, *n* = 758; fibroblasts, *n* = 164). ***, P < 0.001, Mann-Whitney test. **(D)** Immunoblot analysis of cell extracts from the WT and genome-edited (CLTA-TagRFP-T/DNM2-EGFP; CD) hESC line and the NPCs and fibroblasts derived from it.

spatial dynamics, obscuring the ability to definitively determine the healthy physiological cell phenotype. To circumvent these problems, we genome-edited a parent human embryonic stem cell (hESC) line to express fluorescent protein fusions of CME proteins at endogenous levels, and differentiated them into different cell types, allowing us to compare CME dynamics and morphology in isogenic cells of distinct differentiated states. We made in-frame fusions of TagRFP-T and EGFP to the genes encoding clathrin light chain A (CLTA) and dynamin2 (DNM2), respectively, using zinc-finger nucleases (ZFNs) and CRISPR/Cas9, respectively (Fig. 1 A). We determined that both clathrin alleles were successfully targeted, whereas only one DNM2 allele was tagged. Clathrin protein expression levels were similar in the genome-edited hESCs as compared with nonedited parental cells, whereas we observed an ~50% reduction in dynamin protein levels in the edited cells compared with the parental cells (Fig. 1 D). Taking advantage of the pluripotent property of the hESCs, we differentiated them into two cell types, fibroblasts, a cell type derived from the mesoderm, and neuronal progenitor cells (NPCs), a cell type derived from the ectoderm (Fig. 1, A and D).

Next, we quantitatively analyzed CME dynamics in the three cell types by combining total internal reflection fluorescence microscopy (TIRFM) with automated particle tracking using a two-color association program (Aguet et al., 2013; Hong et al., 2015). As dynamin is recruited near the end of the CME pathway and marks release of the vesicle from the PM, only clathrin tracks joined by dynamin were considered to represent bona fide CME events, as opposed to CCVs derived from other membranes and "visiting" the TIRFM field (Hong et al., 2015).

Our analyses showed dramatic differences in endocytic dynamics between the three cell types. In hESCs, clathrin mostly appeared as diffraction-limited spots that recruited dynamin (Fig. 1 B and Video 1). Larger, more static structures were less frequent. By comparison, large, apparently static, clathrin structures were more prominent in fibroblasts (Video 2). Interestingly, although the clathrin structures in the fibroblasts appeared stable, dynamin was repeatedly recruited to their edges, and we observed the apparent formation and release of CCVs from the structures (arrowhead in Video 2). These observations indicate that these long-lived clathrin

structures produce CCVs, as has been described in neurons (Rosendale et al., 2017), HEK293 cells (Lampe et al., 2014), and NIH3T3 cells (Taylor et al., 2012). In NPCs, however, clathrin and dynamin appeared only as dynamic, discrete colocalized puncta. Their lifetimes—defined as the time the proteins are present on the PM—were significantly shorter. The lifetimes of clathrin and dynamin were 40 ± 1 and 30 ± 1 s, respectively, for NPCs, as compared with 75 ± 2.5 and 45 ± 2, or 65 ± 3 and 50 ± 3 s, in hESCs and fibroblasts, respectively (mean ± SEM; Fig. 1 C and Video 3). As a consequence of this highly dynamic, uniform behavior, the productivity, defined as the number of clathrin tracks associated with dynamin per time per area, was much greater in NPCs as compared with hESCs and fibroblasts (0.05 ± 0.005 compared with 0.02 ± 0.004 and 0.01 ± 0.002 tracks·μm^{-2}·min^{-1}, respectively).

Platinum replica EM of unroofed cells was used to determine the ultrastructure of clathrin at the PM in the three different cell types (Fig. 2 A). We categorized clathrin structures as flat, curved, or spherical, corresponding to the stages of CME, as defined previously (Sochacki et al., 2017; Fig. 2 A). In both the hESCs and NPCs, as expected, we observed mainly spherical structures with a similar size (Fig. 2 C). No flat structures were observed in NPCs. In hESCs, the flat structures were small and likely represent the CCP initiation stage (Fig. 2, A–C). Of note, EM images revealed a dense actin cortex in both hESCs and NPCs, which might cover some flat structures, causing us to underestimate their occurrence (full image of these cells in Figs. S1 and S2). In fibroblasts, the flat and curved clathrin structures were dramatically different: the curved clathrin structures were about two times larger and asymmetric, and occasionally clustered together (Fig. 2, A–D; and Fig. S3). These interesting structures correlate well with observations in TIRFM, where clathrin appeared first as large structures that gave rise to several smaller structures when DNM2 was recruited. The flat structures were often connected to curved and spherical clathrin structures, as previously observed in NIH3T3 fibroblasts (Lampe et al., 2014). Together, these results show that the morphology and dynamics of CME proteins are distinctly specified for each defined cell type.

We next compared rates of endocytic uptake of labeled transferrin (Tf) in the three cell types. Although clathrin appeared to be the least dynamic in fibroblasts, it appeared that these cells internalize more Tf compared with hESCs and NPCs (Fig. 2 E). However, fibroblasts might express more receptors on the PM. To account for this possibility, we normalized the amount of Tf taken up to the amount of Tf bound to receptors on the cell surface at time 0 (Fig. 2 F). Interestingly, the fraction of the bound material that was internalized was lower in fibroblasts compared with the hESCs and NPCs (Fig. 2 E, right graph). We compared the endocytic uptake rates of Tf in WT (unedited) hESCs and in the genome-edited hESCs and found that the rates were indistinguishable, which indicates that CME is not perturbed in the edited cells.

Collectively, these data show that clathrin lattice structures on the PM are remodeled during stem cell differentiation and that the endocytic internalization process is differentiated between the three cell types.

AP2 regulates CCS dynamics and size

Because each cell type is characterized by a specific gene expression pattern, and because our model avoids genetic variability, we made in-frame fusions of tagGFP2 to the gene encoding the μ2 subunit of the clathrin adaptor AP2, as described previously (Fortian et al., 2015; Hong et al., 2015). As we differentiated the hESCs into fibroblasts and NPCs, we found that AP2 levels at endocytic sites changed during differentiation to these two cell types. The AP2 levels at endocytic sites decreased threefold in NPCs compared with hESCs, and increased twofold in fibroblasts compared with hESCs (Fig. 3 A and Video 4). Interestingly, AP2μ2 expression levels were similar in hESCs and NPCs, but were elevated in fibroblasts (Figs. 1 D and 3 B). We hypothesized that AP2μ2 expression levels might influence CME site structure and dynamics, especially because experimental lowering of AP2 levels previously was shown to reduce CCV diameter (Miller et al., 2015). To test this hypothesis, we partially depleted AP2μ2 using a validated siRNA (Boucrot et al., 2015) in fibroblasts (Fig. 3, C–E; and Video 5). In AP2μ2-depleted fibroblasts, the large clathrin structures disappeared (Fig. 3 C). In addition, clathrin lifetimes decreased (60 ± 0.6 s in AP2-depleted cells compared with 80 ± 1.6 s in control cells; Fig. 3 D), and we observed a dramatic increase in CME productivity (Fig. 3 E). Together, these results reveal that during fibroblast differentiation, AP2 expression levels increase, which contributes to formation of the large, static clathrin structures. Likewise, we infer that reduction of AP2 expression during NPC differentiation promotes formation of uniformly small and highly dynamic CME sites. To regulate endocytic dynamics and structure, the cell finely tunes the expression of core CME components.

Actin functions in CME in a cell type–dependent manner

In platinum replica EM, we observed that all clathrin structures, even the flat structures in hESCs and NPCs, were associated with actin filaments, as observed previously in mouse melanoma cells (Collins et al., 2011; Fig. 2 A). In mammalian cells, different effects of actin depolymerizing and stabilizing drugs on CME dynamics have been observed in different cell lines and cell contexts, showing a disparity in the actin requirement for CME (Fujimoto et al., 2000; Yarar et al., 2005; Brady et al., 2010; Boulant et al., 2011; Cheng et al., 2012; Taylor et al., 2012; Grassart et al., 2014). Here, to determine whether actin dependence is a product of cell fate, we treated the three isogenic cell types with Latrunculin A (LatA) and Jasplakinolide (Jasp), actin depolymerizing and stabilizing drugs, respectively (Videos 6 and 7). We analyzed the effect of these drugs on the CME productivity, clathrin and dynamin lifetimes, and CCP stabilization (Fig. 4, A and B; Fig. S4, A–C; and Table 1). Dramatic differences in drug effects were observed, which may relate to differences in the actin cortex observed in EM (Figs. S1, S2, and S3) and light microscopy (unpublished data). Overall, endocytosis in hESCs and NPCs responded to LatA treatment similarly: the productivity decreased and clathrin and dynamin were stabilized for most CCPs, with a shorter lifetime when endocytic events were productive. Interestingly, in NPCs, Jasp had the same effects as LatA, except that it did not affect endocytic lifetimes. However, in hESCs, Jasp treatment resulted in a twofold increase in CME productivity as well as a slight
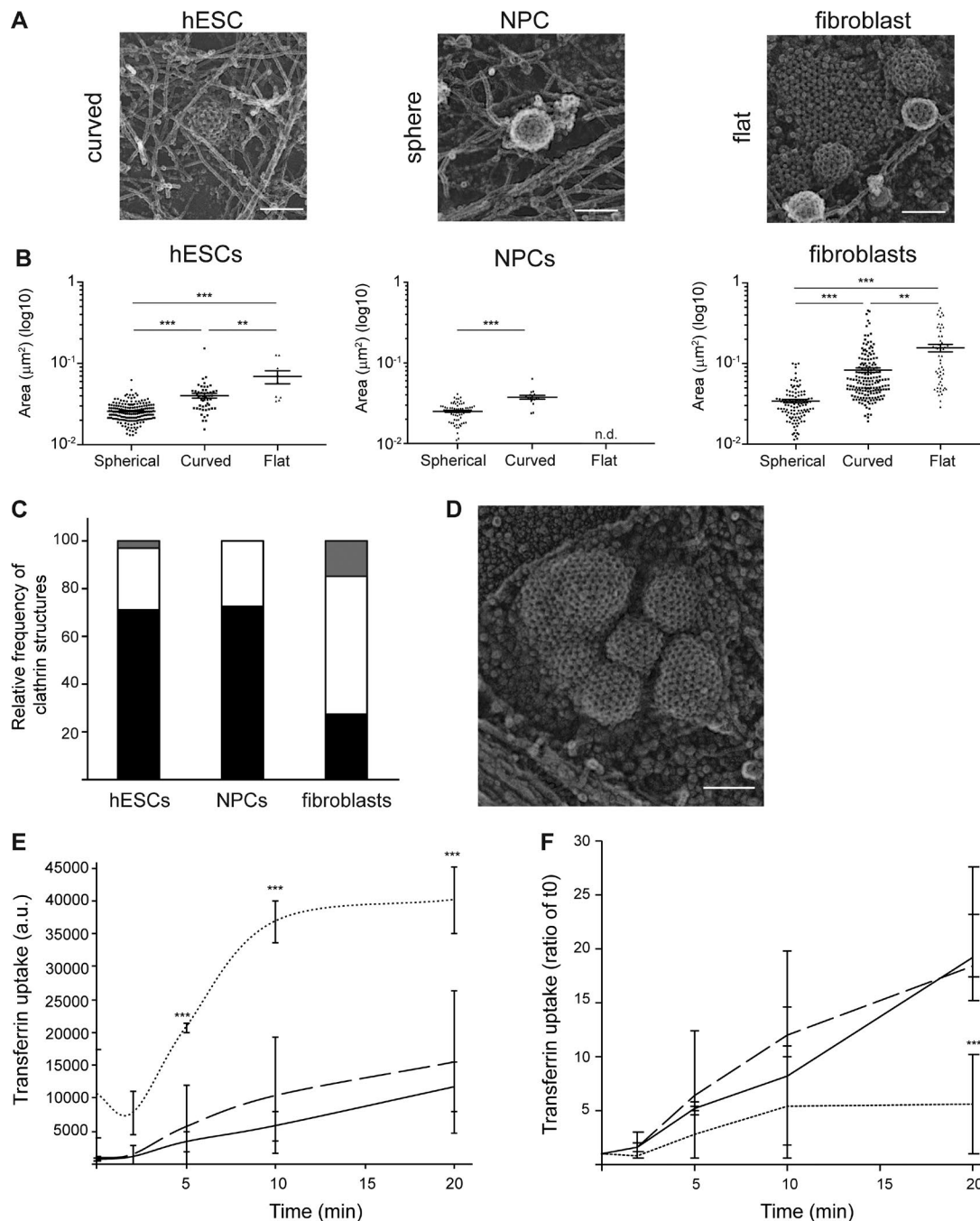
Dambournet et al.
Clathrin-mediated endocytosis in differentiation

Journal of Cell Biology
https://doi.org/10.1083/jcb.201710084

3303

Figure 2. **Ultrastructure of clathrin lattices in the three cell types. (A)** Platinum replicas of representative curved, spherical, and flat clathrin structures in hESCs, NPCs, and fibroblasts, respectively. Bars, 200 nm. **(B)** Area of clathrin structures in the three different cell types (mean ± SEM). ***, P < 0.001; **, P < 0.01; Mann-Whitney test (three to four replicas, total number of structures analyzed: hESCs, n = 245; NPCs, n = 100; fibroblasts, n = 337). **(C)** Relative frequency of spherical (black), curved (white) and flat (gray) clathrin structures in hESCs, NPCs, and fibroblasts (three to four replicas, total number of structures analyzed: hESCs, n = 245; NPCs, n = 100; fibroblasts, n = 337). **(D)** Representative EM micrograph showing clustering of curved clathrin structures in fibroblasts. Bar, 200 nm. **(E and F)** Tf uptake in hESCs (black line), NPCs (dashed line), and fibroblasts (dotted line). For each time point, at least 2,000 cells were analyzed. Fluorescently labeled Tf levels were measured by flow cytometer (mean ± SD). ***, P < 0.001; **, P < 0.01; unpaired two-tailed t tests (three to four independent experiments, n = 2,000 cells) (F) Normalized amount of Tf uptake relative to the amount of Tf bound to the receptor at the cell surface at time 0 (mean ± SD). ***, P < 0.001; unpaired two-tailed t test (three to four independent experiments, n = 2,000 cells per experiment).

increase in clathrin and dynamin lifetimes, but it did not stabilize CCPs. In contrast, in fibroblasts, clathrin and dynamin lifetimes were unaffected by LatA and Jasp treatment, but LatA resulted in an increase in CME productivity, whereas Jasp treatment dramatically increased the number of large clathrin structures and

stabilized CCPs (Fig. S4 D, Fig. 4 C, and Table 1). The variety of effects of the actin drugs on the different cell types indicates that actin performs different functions at different stages of CME in the different cell types. In NPCs, actin is required for vesicle scission by DNM2, as found previously in some tissue culture cells
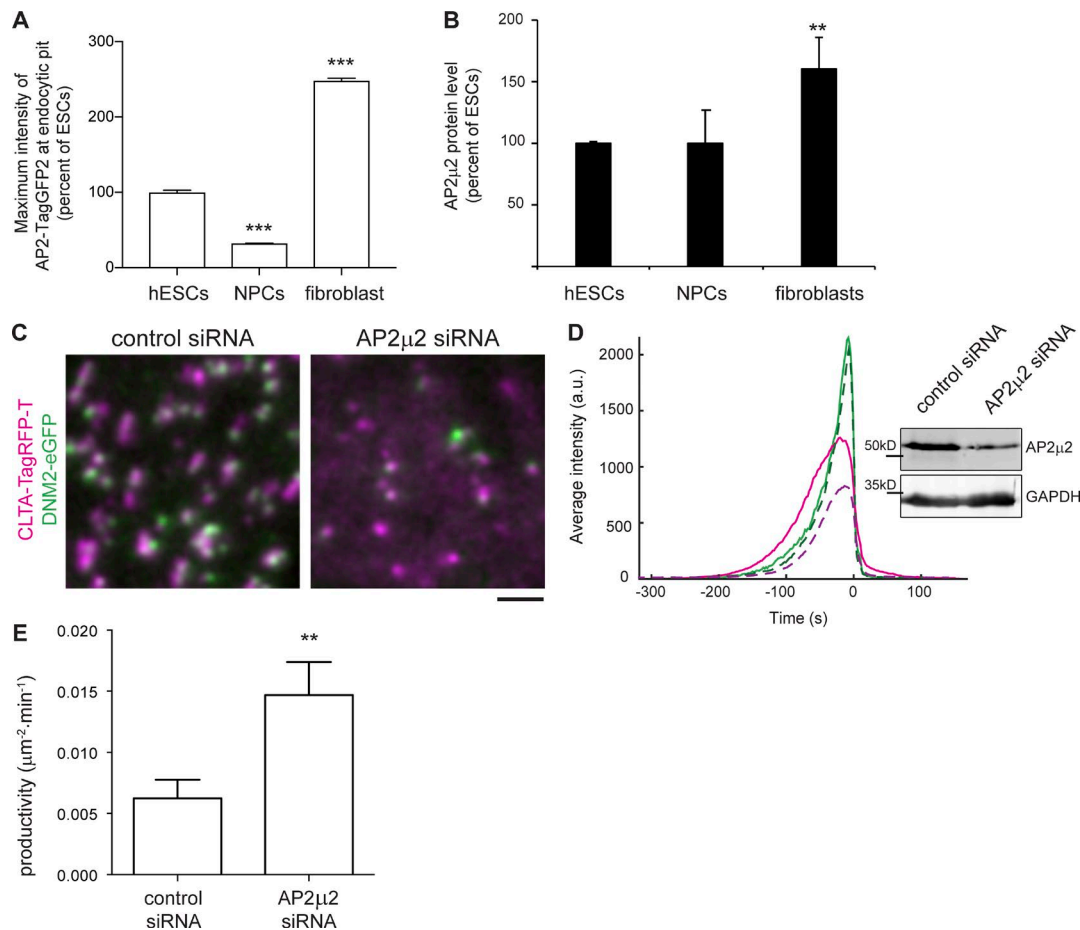
Figure 3. **Large clathrin structures are lost from fibroblasts upon AP2μ2 depletion. (A)** Maximum intensity of AP2-TagGFP2 at endocytic site in hESCs, NPCs, and fibroblasts relative to hESCs (mean ± SEM). ***, P < 0.001, Mann-Whitney test (three to eight cells analyzed, 600–10,000 tracks analyzed). **(B)** Quantification of AP2μ2 expression levels in the three cell types. AP2μ2 levels were analyzed by immunoblot and normalized to the loading control (mean ± SD). **, P < 0.01, unpaired two-tailed t tests (three independent experiments). **(C)** Representative TIRFM images of CLTA-TagRFP-T (magenta) and DNM2-EGFP (green) in fibroblast transfected with control or AP2μ2 siRNA. Bar, 2 μm. **(D)** Mean fluorescence intensity profile for CLTA-TagRFP-T (magenta line for control cells and dark magenta dashed line for AP2μ2 siRNA) and DNM2-EGFP (light green line for control cells and dark green dashed line for AP2μ2 siRNA) in fibroblasts transfected with control or AP2μ2 siRNA (four independent experiments, three to four cells analyzed per experiment, 1,000–2,600 tracks analyzed) Western blot analysis of cell lysates immunoblotted for AP2μ2 and GAPDH loading control. **(E)** Endocytic productivity in fibroblasts transfected with control or AP2μ2 siRNA (mean ± SEM). **, P < 0.01, one-way ANOVA and Dunnett's test versus control (four independent experiments, three to four cells analyzed per experiment, 1,000–2,600 tracks analyzed). ESC, embryonic stem cell.

(Boulant et al., 2011; Taylor et al., 2012; Grassart et al., 2014). In hESCs, however, actin was required for both early and late stages of CME. However, Jasp treatment increased CME productivity, perhaps through the stabilization of short actin filaments that could recruit actin-binding endocytic proteins or aid in Arp2/3 activation at early stages of CME (Bubb et al., 2000). In fibroblasts, we observed that the large clathrin structures are often close to focal adhesions (unpublished data). The effect of actin drugs in fibroblasts might therefore be associated with the stabilization of focal adhesions in LatA- and Jasp-treated cells (Zamir et al., 2000; Hoffman et al., 2006), although the increase in CME productivity in LatA-treated fibroblasts might result from destabilization of clustered curved clathrin structures.

Phosphoinositide (PI)-3 kinase modulates receptor-mediated endocytosis

We hypothesized that rewiring of signal transduction pathways during cell differentiation leads to differences in cell signaling

that contribute to the distinct CME site structures and dynamics for each of the three cell types. The PI-3 kinase pathway is associated with activation and signaling of a variety of receptors including EGF receptor and G-protein–coupled receptors (Sorkin and von Zastrow, 2009). We treated each of the cell types with the PI-3 kinase inhibitor LY294002 (LY; Gharbi et al., 2007) and observed dramatic differences (Fig. 5 A, Video 8, and Table 1). In all three cell types, LY treatment induced a dramatic decrease in clathrin and dynamin lifetimes at the PM for the dynamic CME sites (Fig. 5 D). In hESCs, but not NPCs or fibroblasts, we also observed a twofold increase in the occurrence of stabilized CCPs, though not a decreased CME productivity (Fig. 5, B and C). Interestingly, the effects of PI-3 kinase inhibition in hESCs are similar to those reported after depletion of the PI-3 kinase C2α in Cos7 cells (Posor et al., 2013). In NPCs, the CME productivity decreased dramatically, whereas it increased in fibroblasts. Here, our results establish that the requirement for PI-3 kinase in CCP maturation differs between the three different isogenic

Dambournet et al.
Clathrin-mediated endocytosis in differentiation

Journal of Cell Biology
https://doi.org/10.1083/jcb.201710084

3305

Table 1. Differential effect of drugs on the three cell types

	Jasplakinolide			LatA			LY		
	Lifetime	CME productivity	CCS stabilized	Lifetime	CME productivity	CCS stabilized	Lifetime	CME productivity	CCS stabilized
hESCs	+	+	No effect	–	–	+	–	No effect	+
NPCs	No effect	–	+++	–	–	+	–	–	+
Fibroblasts	No effect	No effect	+++	–	+	+	–	+	No effect

Table summarizes the different effect of actin and PI-3 kinase drugs on CME of the three cell types. + and – indicate, respectively, an increase or a decrease of the corresponding parameters compared to control condition.

cell types. Because downstream effectors of the PI-3 kinase pathway have recently been shown to play an important role in CME (Liberali et al., 2014; Reis et al., 2015), future studies are required to determine which of the downstream effectors or lipid modifications affect CME in each cell type, and whether the differential effects observed are a result of differences in PI-3 kinase isoforms present in the three cell types or indirect effects at other trafficking steps, such as at endosomes.

Discussion

As cells differentiate, essentially every aspect of their physiology and structure becomes adapted to their new state. To date, studies have almost exclusively focused on the gene expression changes that underlie differentiation rather than on how cell structure and function are adapted. Here, we used genome-edited human stem cells to study how cellular processes are altered during differentiation in isogenic cells. We genome-edited hESCs and used cell differentiation protocols to create an isogenic set of cells to uncover cell type–specific mechanistic differences in CME. Previously, CME dynamics had been studied in a variety of nonisogenic cell lines representing different cell types and species. These cell lines were almost always derived from cancers and are therefore characterized by chromosome instability and associated phenotypic variation. These uncontrolled variables in cell physiology and structure, and the practice of overexpressing
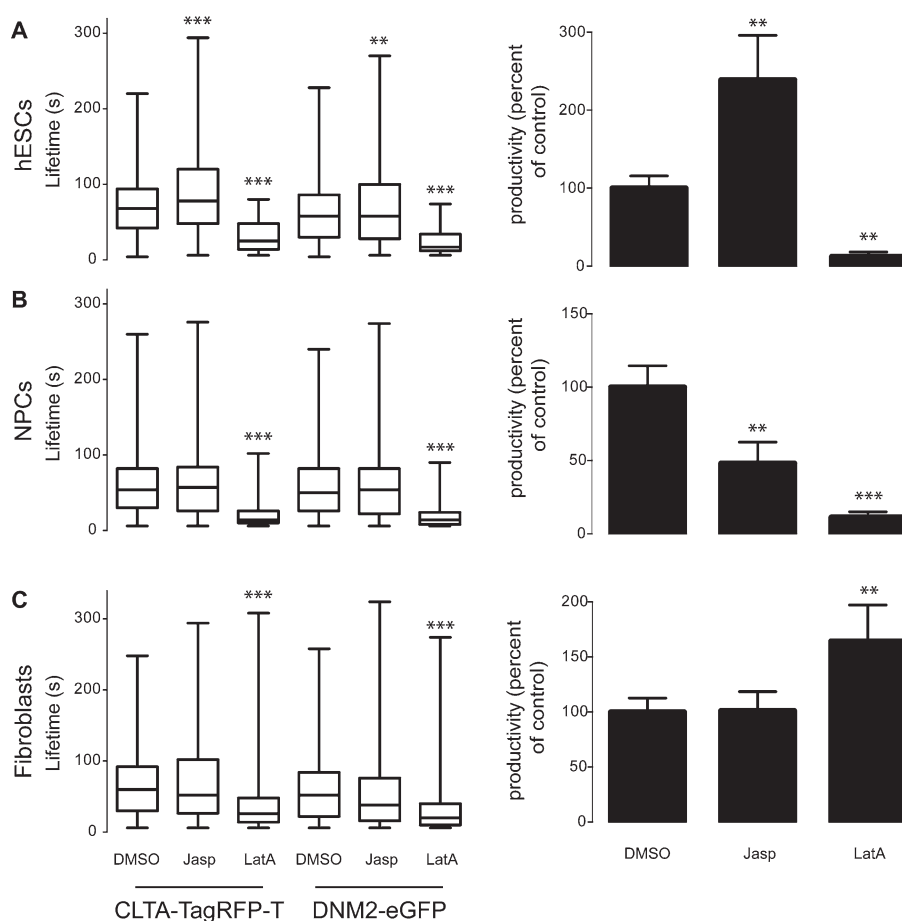

Figure 4. **Actin role in CME varies with cell type.** Clathrin and dynamin lifetimes and productivity of endocytic events in hESCs (A), NPCs (B), and fibroblasts (C) after treatment with DMSO, LatA (1 µM for hESCs and NPCs and 100 nM for fibroblasts), or Jasp (1 µM). Box plots show medians extended from the 25th to 75th percentiles, minimum and maximum data points. ***, P < 0.001, one-way ANOVA and Dunnett's test versus control (five independent experiments, three to four cells analyzed per experiment, 30–800 structures analyzed).

Figure 5. **The PI-3 kinase pathway plays a cell type–specific role in CME. (A)** Representative kymographs of hESCs, NPCs, and fibroblasts treated with DMSO or 1 µM LY for 20 min. CLTA-TagRFP-T (magenta) and DNM2-EGFP (green). Bar, 5 µm. **(B)** Density of stalled events in LY-treated cells relative to respective DMSO-treated cells (mean ± SEM). ***, P < 0.0001, one-way ANOVA and Dunnett's test versus control (five independent experiments, three to four cells analy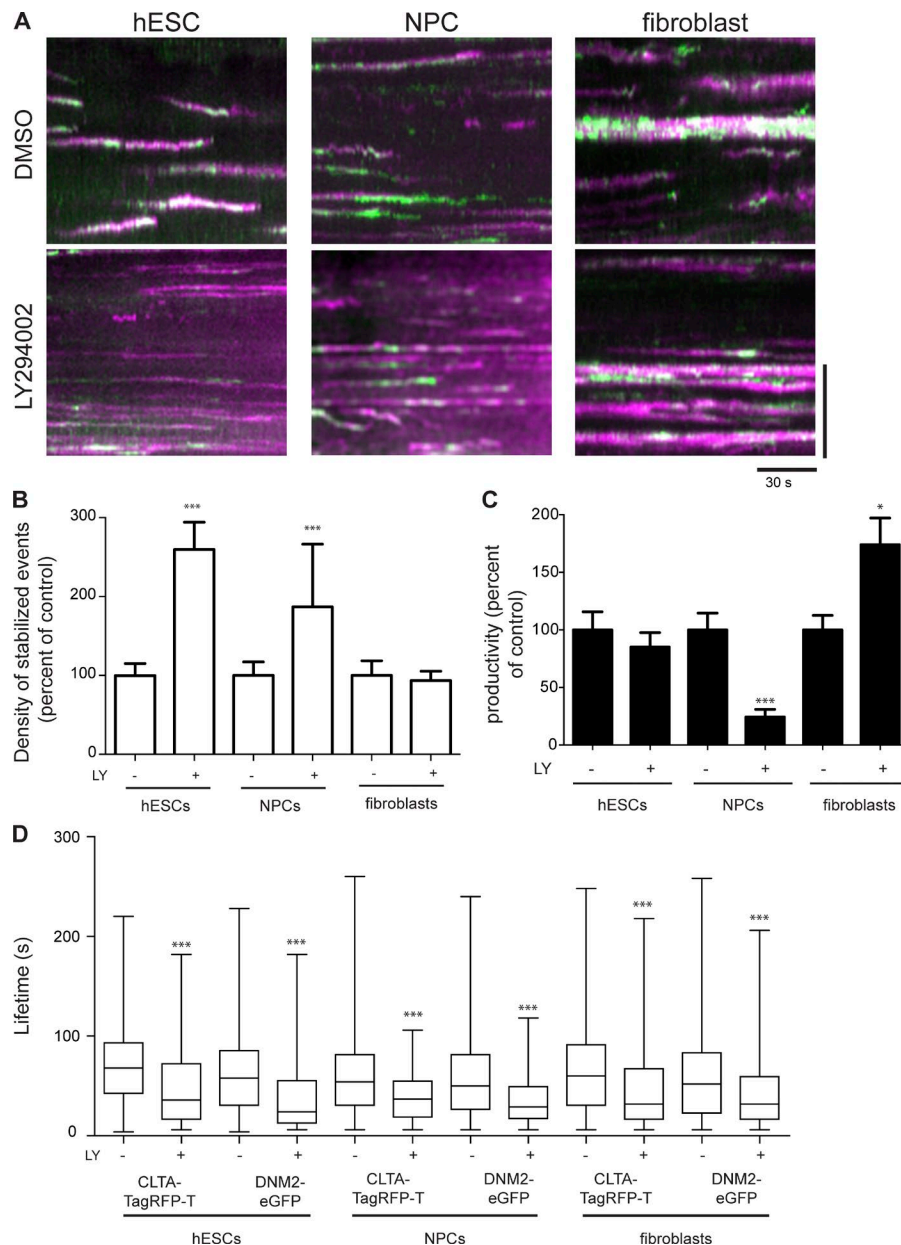zed per experiment, 60–800 structures analyzed). **(C)** Productivity of endocytic events in LY-treated cells relative to respective control cells (mean ± SEM). ***, P < 0.001, one-way ANOVA and Dunnett's test versus control (five independent experiments, three to four cells analyzed per experiment, 60–800 structures analyzed). **(D)** Lifetimes for clathrin and dynamin in hESCs, NPCs, and fibroblasts treated with DMSO or 1 µM LY. Box plots show median lifetimes between the 25th to 75th percentiles. The full range covering the minimum to maximum data points is shown (mean ± SEM). ***, P < 0.001, one-way ANOVA and Dunnett's test versus control (five independent experiments, three to four cells analyzed per experiment, 60–800 structures analyzed).

labeled proteins for imaging studies, have likely contributed significantly to discrepancies in the literature about CME dynamics, morphology, and sensitivity to specific inhibitors. Here, we developed a system that allowed us to determine how various previously made observations fit together in a coherent, physiologically relevant manner as cells differentiate, and to identify the underlying, developmentally regulated basis for establishing the new cell phenotypes.

Clathrin dynamics and morphology are adapted upon cell differentiation

Our use of isogenic cells of three different types for this study enabled us to demonstrate that the ubiquitous process of CME is versatile and can be adapted to the specifications required in each new cell type. Clathrin dynamics are dramatically different in NPCs and fibroblasts, cells that arise from different lineages, ectoderm and mesoderm, respectively, and have different

roles within the body. It is interesting to speculate about why CME might have different characteristics in different cell types. NPCs are highly motile cells that give rise to neurons and glial cells, both of which produce highly elongated structures during differentiation. Perhaps extensive PM remodeling by dynamic CME is required for high cell motility and/or production of the elongated structures. In contrast, fibroblasts have low motility and interact tightly with the extracellular matrix through focal adhesions. Focal adhesions are known to participate in formation and stabilization of large clathrin plaques (Ezratty et al., 2009; Saffarian et al., 2009). Furthermore, fibroblasts respond to chemical and mechanical signals during wound healing and can be differentiated into specialized cells depending on substrate stiffness (Engler et al., 2006). Interestingly, clathrin plaques are suggested to serve as hubs for cell signaling by specific receptors such as LPAR (lysophosphatidic acid receptor; Leyton-Puig et al., 2017). These observations raise the possibility that in fibroblasts,

large clathrin plaques sense mechanochemical cues for efficient cellular responses.

Recently different clathrin assembly models have been proposed: a constant curvature model, a constant area model, and a flat-to-curved transition model, which depends on the AP2/clathrin ratio (Heuser, 1980; Avinoam et al., 2015; Lampe et al., 2016; Bucher et al., 2018). Interestingly, we found in isogenic cells that clathrin ultrastructure varies dramatically from one cell type to another. Based on our results, it seems that the propensity for clathrin structures to evolve from flat to curved structures may be different in fibroblasts compared with hESCs or NPCs. In NPCs, clathrin structures appear to start as small, flat structures, with the coat area growing as the curvature of the future vesicle increases. This observation is consistent with the models proposed by Bucher et al. (2018) and Scott et al. (2018). However, in fibroblasts, most of the flat structures are larger and are connected to domed and/or spherical structures (Fig. 2, B and D). These structures raise the possibilities that either new clathrin molecules are recruited at the edge of these flat structures, where they assemble directly into curved structures, or the flat clathrin lattice rearranges into curved structures. Another possibility is that "activation" of the AP2 complex, by sufficient loading of AP2-bound receptors within the clathrin lattice, induces a change in conformation of clathrin, and then the bending of the PM (Dannhauser and Ungewickell, 2012; Dannhauser et al., 2015; Kadlecova et al., 2017; Fig. 2 D). These two possibilities are not exclusive, as it has been proposed recently that membrane bending can occur either as clathrin assembles at the PM or after its assembly (Scott et al., 2018).

Because optimal growth conditions (media and substrate) differ for each cell type, it was possible that differences observed were a result of these differences rather than the distinct differentiated states of the cells. In fact, the growth conditions and differentiated states are intimately connected. Nevertheless, we did grow fibroblasts on matrigel and in separate experiments tested mTESR medium on the fibroblasts, and observed similar dynamics and morphology compared with growth in the normal media and on their normal substrate.

AP2 levels at CME sites dictate CCV architecture and dynamics

Our studies revealed that differentiation is accompanied by a dramatic change in AP2 expression. We found that AP2 is up-regulated during fibroblast differentiation and is elevated compared with hESCs and NPCs. Our knockdown study provided direct evidence that elevated AP2 levels are responsible of the formation of large clathrin plaques, as knocking down AP2 expression eliminated plaques and increased dynamics. The presence of smaller, more highly curved clathrin structures in NPCs, which have significantly lower AP2 levels, seems consistent with the idea posited by Bucher et al. (2018) that curvature is promoted by higher clathrin/AP2 ratios and the demonstration by Miller et al. (2015) that lower AP2 levels decrease CCV diameter. Although AP2 is a key component of the endocytic machinery, it is likely that additional endocytic proteins are differentially regulated during differentiation into different cell types. Thus, further studies will be needed to identify the components responsible for the dynamics differences between the hESCs and the NPCs,

especially because, based on the differential drug sensitivity, we hypothesize that the actin cytoskeleton might play an unexpected role during early stages of CME in hESCs.

A general approach for investigation of how cellular processes are adapted during differentiation

Pluripotent stem cells have the ability to differentiate into essentially any cell type, offering an opportunity to determine how cellular processes become adapted for the functions and properties of different cell types. Studies of how cellular processes are modified during stem cell differentiation eliminate confounding effects caused by genetic variability and chromosome instability because the resulting cells are isogenic, have normal physiology, and have normal karyotypes. This approach allowed us to discover programmed changes in protein expression and endocytic site ultrastructure and dynamics. Furthermore, the insertion of a fluorescent protein coding sequence at the endogenous locus in stem cells by genome editing eliminates cell-to-cell expression variability and overexpression effects caused by random plasmid integration. Extension of this approach promises to make possible determination of how many additional cellular processes are adapted during differentiation, and to identify the key factors involved.

Materials and methods

Cell culture

hESCs (WIBR3, National Insitutes of Health stem cell registration 0079) were cultured as previously described (Soldner et al., 2009; Hockemeyer et al., 2011). In brief, hESCs were maintained on a layer of inactivated mouse embryonic fibroblasts in hESC medium (DMEM/F12; Lifetech) supplemented with 20% Knock-Out Serum Replacement (Lifetech), 1 mM glutamine (Lifetech), 1% nonessential amino acids (Lifetech), 0.1 mM β-mercaptoethanol (Sigma-Aldrich), 1,000 U/ml penicillin/streptomycin (Lifetech), and 4 ng/ml FGF2 (Lifetech). Cultures were passaged every 7 d with collagenase type IV (1.5 mg/ml; Lifetech) and gravitational sedimentation by washing three times in wash medium (DMEM/F12; Lifetech) supplemented with 5% fetal bovine serum (Lifetech), and 1,000 U/ml penicillin/streptomycin (Lifetech). Cell lines were tested for mycoplasma infection every month.

Differentiation into NPCs and fibroblasts

hESCs were differentiated into NPCs and fibroblasts as previously described (Chiba et al., 2015).

NPC differentiation

Cells were cultured under feeder free conditions on matrigel-coated plates in mTESR1 medium (Stem Cell Technologies). The dual SMAD inhibition protocol for the differentiation of hESCs into NPCs was adapted from Chambers et al. (2009). In brief, hESCs were cultured for 10 d with increasing amounts of N2 medium (50% DMEM/F12; Lifetech), 50% Neurobasal Medium (Lifetech), 0.75% BSA (wt/vol; Sigma-Aldrich), N2 Supplement (Lifetech), 20 ng/ml insulin (Sigma-Aldrich), 1 mM glutamine (Lifetech), 1,000 U/ml penicillin/streptomycin (25%, 50%, 75%; Lifetech) supplemented with KOSR medium (hESC medium without FGF),

Dambournet et al.
Clathrin-mediated endocytosis in differentiation

Journal of Cell Biology
https://doi.org/10.1083/jcb.201710084

3308

100 ng/µl Noggin (R&D Systems), and 10 µM SB431542 (Tocris). NPCs were maintained in N2 medium supplemented with 25 ng/ml FGF2 (Lifetech) and 40 ng/ml EGF (R&D Systems).

Fibroblast differentiation

For the formation of embryonic bodies, hESC colonies were grown on ultralow attachment plates (Corning) in fibroblast medium (DMEM/F12; Lifetech) supplemented with 15% fetal bovine serum (Lifetech), 1 mM glutamine (Lifetech), 1% nonessential amino acids (Lifetech), and penicillin/streptomycin (Lifetech). After 9 d, embryonic bodies were transferred to tissue culture dishes coated with 0.2% gelatin and maintained in fibroblast medium (Ahfeldt et al., 2012).

Gene targeting in hESCs

Cas9 and single guide RNAs were expressed using the pX330 plasmid (Cong et al., 2013; Ran et al., 2013). The *CLTA* genes were targeted as previously described using a paired ZFN that targets exon 7 and cuts precisely at the stop codon (Doyon et al., 2011; Hong et al., 2015). TALENs targeted exon 7 and were designed to cut the AP2M1 gene locus at a site corresponding to residue 236 of the AP2 µ subunit (Hong et al., 2015). The design of donor plasmids and ZFNs was described previously (Doyon et al., 2011). The *DNM2* gene was targeted at exon 22 using CRISPR/Cas9 and 5′-CCTGCTCGACTAGGCCTCGA-3′ as a guide RNA, which cuts in the immediate vicinity of the stop codon. 1–2 × 10^7 hESCs were electroporated with 5 µg of each ZFN/TALEN (or 10 µg of pX330 Cas9 plasmid) and 40 µg of donor plasmid. Cells were sorted out by an Influx sorter (BD Bioscience) for GFP and/or RFP fluorescence 72 h after electroporation. Clonal populations were isolated and characterized as previously described (Dambournet et al., 2014).

TIRFM and live-cell imaging

48 h before imaging, hESCs and NPCs were seeded onto Matrigel-coated glass coverslips and fibroblasts onto gelatin-coated coverslips. TIRFM images were captured using Meta-Morph software on an Olympus IX-81 microscope outfitted with an APON 60×/1.49 NA TIRFM oil objective and an ORCA-R2 camera (Hamamatsu Photonics). Cells were imaged in their appropriate media and kept at 37°C during imaging. A DV2 image splitter (MAG Biosystems) was used to separate GFP and RFP emission signals. Time-lapse videos were obtained with 500-ms exposure times, at 2-s intervals, and with 4–6-min duration.

Tf uptake assay using a flow cytometer

The Tf endocytosis assay was modified from Grassart et al. (2014). In brief, hESCs, NPCs, and fibroblasts were seeded on a 24-well plate 2 d before the analysis. After 30 min in serum starvation medium (HBSS + BSA), cells were incubated with 20 µg/ml Tf–Alexa Fluor 647 at 37°C. Cells were then transferred to ice, and surface-bound Tf–Alexa Fluor 647 was removed using ice-cold acid buffer (HBSS, 0.5% acetic acid, and 0.5 M NaCl) for 45 s. The cell culture medium was then neutralized by extensive washes with DMEM-BSA. Cells were collected using EDTA-Trypsin, washed, and fixed in cold 4% PFA. Intracellular fluorescence of Tf–Alexa Fluor 647 was quantified by a flow cytometer (LSR Fortessa; BD Bioscience). Results in Fig. 1 F were normalized to the surface expression of Tf receptor, evaluated by incubation of the cells with Tf–Alexa Fluor 647 on ice for 30 min.

Drug perturbations

Before imaging, cells were treated with appropriate culture media containing 0.01% (vol/vol) DMSO, 1 µM Jasp, 0.1–1 µM LatA, or 10 µM LY. Of note, fibroblasts were more sensitive than NPCs and hESCs to LatA treatment, so we used 100 nM LatA instead of 1 µM, consistent with previous findings that LatA has a dose-dependent effect on endocytosis (Grassart et al., 2014).

Image analysis

We tracked the positions of the fluorescent spots in each channel over time using the detection and tracking portions of the cmeAnalysis software (Aguet et al., 2013). We wrote a script in Matlab to extract the x-y coordinates for use in a custom-written program that associates, classifies, and plots corresponding GFP and RFP tracks (Hong et al., 2015). Only clathrin- and DNM2-associated tracks were considered as bona fide endocytic events. Track output was then inspected individually to correct for association errors. Only tracks that appeared and disappeared during the lifetime of the acquisition (i.e., 121 frames, 4 min) were subjected to lifetime analyses. The programs are available for download in the online supplemental material.

Unroofing and EM

Cells were prepared as described for live-cell imaging. Cells were washed in stabilization buffer (70 mM KCl, 30 mM Hepes, pH 7.4, 5 mM MgCl$_2$, and 3 mM EGTA [all from Sigma-Aldrich]). The cells were then unroofed using a 10-ml syringe with a 22-gauge, 1.5-in needle with 2% PFA (EM Sciences) diluted in stabilization buffer. Cells were then transferred and fixed for 20 min in 2% glutaraldehyde (EM Sciences). Transmission EM of platinum cell membrane replicas was performed as previously described (Sochacki et al., 2017).

RNAi and Western blot experiments

Fibroblasts were transfected with the corresponding siRNA using Lipofectamine 2000 (Invitrogen) following the manufacturer's instructions. A nontargeting siRNA pool (siRNA control; ON-TARGETplus SMARTpool siRNA 4; Thermo Fisher Scientific; Grassart et al., 2014) and Stealth HSS101955 against AP2µ2 (Invitrogen; Boucrot et al., 2015) were used for depletion experiments. RNAi knockdown efficiency was verified by Western blot, and cells were imaged 72 h after transfection. Cells were lysed in lysis buffer (50 mM Hepes, pH 7.4, 150 mM NaCl, 1 mM MgCl$_2$, 0.1% Triton X-100, and protease inhibitor) and loaded onto an acrylamide gel for SDS-PAGE followed by immunoblotting. Blots were incubated for 1 h at room temperature or overnight at 4°C with primary antibodies and subsequently incubated in the dark at room temperature with secondary antibodies. Membranes were scanned on an Odyssey infrared imager (LI-COR Biosciences). Quantification of protein bands was performed using Image Studio (version 3.1).

Online supplemental material

Figs. S1, S2, and S3 show a representative EM replica of hESC, NPC, and fibroblast cells, respectively. Fig. S4 shows the

differential effect of actin drugs on the three cell types. Videos 1, 2, and 3 show TIRFM time-lapse video (4 min) of the hESC (hCLTA^{EN}/DNM2^{EN}), hNPC, and fibroblast, respectively. Video 4 shows TIRFM time-lapse videos (4 min) of the hESC (AP2-tag-GFP2), hNPC, and fibroblast. Video 5 represents TIRFM time-lapse videos (4 min) of control and AP2μ2-depleted fibroblasts. Video 6 represents TIRFM time-lapse videos (6 min) of the hESC (hCLTA^{EN}/DNM2^{EN}), hNPC, and fibroblasts treated with LatA. Video 7 shows TIRFM time-lapse videos (4min) of the hESC (hCLTA^{EN}/DNM2^{EN}), hNPC, and fibroblasts treated with Jasp. Video 8 represents TIRFM time-lapse videos (4 min) of the hESC (hCLTA^{EN}/DNM2^{EN}), hNPC, and fibroblasts treated with LY. Table S1 shows a list of reagents. The image analysis programs used in this study are available for download as a ZIP file.

Acknowledgments

References

Aguet, F., C.N. Antonescu, M. Mettlen, S.L. Schmid, and G. Danuser. 2013. Advances in analysis of low signal-to-noise images link dynamin and AP2 to the functions of an endocytic checkpoint. *Dev. Cell.* 26:279–291. https://doi.org/10.1016/j.devcel.2013.06.019

Ahfeldt, T., R.T. Schinzel, Y.-K. Lee, D. Hendrickson, A. Kaplan, D.H. Lum, R. Camahort, F. Xia, J. Shay, E.P. Rhee, et al. 2012. Programming human pluripotent stem cells into white and brown adipocytes. *Nat. Cell Biol.* 14:209–219. https://doi.org/10.1038/ncb2411

Avinoam, O., M. Schorb, C.J. Beese, J.A.G. Briggs, and M. Kaksonen. 2015. END OCYTOSIS. Endocytic sites mature by continuous bending and remodeling of the clathrin coat. *Science.* 348:1369–1372. https://doi.org/10.1126/science.aaa9555

Boucrot, E., A.P.A. Ferreira, L. Almeida-Souza, S. Debard, Y. Vallis, G. Howard, L. Bertot, N. Sauvonnet, and H.T. McMahon. 2015. Endophilin marks and controls a clathrin-independent endocytic pathway. *Nature.* 517:460–465. https://doi.org/10.1038/nature14067

Boulant, S., C. Kural, J.-C. Zeeh, F. Ubelmann, and T. Kirchhausen. 2011. Actin dynamics counteract membrane tension during clathrin-mediated endocytosis. *Nat. Cell Biol.* 13:1124–1131. https://doi.org/10.1038/ncb2307

Brady, R.J., C.K. Damer, J.E. Heuser, and T.J. O'Halloran. 2010. Regulation of Hip1r by epsin controls the temporal and spatial coupling of actin filaments to clathrin-coated pits. *J. Cell Sci.* 123:3652–3661. https://doi.org/10.1242/jcs.066852

Bubb, M.R., I. Spector, B.B. Beyer, and K.M. Fosen. 2000. Effects of jasplakinolide on the kinetics of actin polymerization. An explanation for certain in vivo observations. *J. Biol. Chem.* 275:5163–5170. https://doi.org/10.1074/jbc.275.7.5163

Bucher, D., F. Frey, K.A. Sochacki, S. Kummer, J.-P. Bergeest, W.J. Godinez, H.-G. Kräusslich, K. Rohr, J.W. Taraska, U.S. Schwarz, and S. Boulant. 2018. Clathrin-adaptor ratio and membrane tension regulate the flat-to-curved transition of the clathrin coat during endocytosis. *Nat. Commun.* 9:1109. https://doi.org/10.1038/s41467-018-03533-0

Chambers, S.M., C.A. Fasano, E.P. Papapetrou, M. Tomishima, M. Sadelain, and L. Studer. 2009. Highly efficient neural conversion of human ES and iPS cells by dual inhibition of SMAD signaling. *Nat. Biotechnol.* 27:275–280. https://doi.org/10.1038/nbt.1529

Cheng, J., A. Grassart, and D.G. Drubin. 2012. Myosin 1E coordinates actin assembly and cargo trafficking during clathrin-mediated endocytosis. *Mol. Biol. Cell.* 23:2891–2904. https://doi.org/10.1091/mbc.e11-04-0383

Chiba, K., J.Z. Johnson, J.M. Vogan, T. Wagner, J.M. Boyle, and D. Hockemeyer. 2015. Cancer-associated TERT promoter mutations abrogate telomerase silencing. *eLife.* 4:693. https://doi.org/10.7554/eLife.07918

Collins, A., A. Warrington, K.A. Taylor, and T. Svitkina. 2011. Structural organization of the actin cytoskeleton at sites of clathrin-mediated endocytosis. *Curr. Biol.* 21:1167–1175. https://doi.org/10.1016/j.cub.2011.05.048

Cong, L., F.A. Ran, D. Cox, S. Lin, R. Barretto, N. Habib, P.D. Hsu, X. Wu, W. Jiang, L.A. Marraffini, and F. Zhang. 2013. Multiplex genome engineering using CRISPR/Cas systems. *Science.* 339:819–823. https://doi.org/10.1126/science.1231143

Dambournet, D., S.H. Hong, A. Grassart, and D.G. Drubin. 2014. Tagging endogenous loci for live-cell fluorescence imaging and molecule counting using ZFNs, TALENs, and Cas9. *Methods Enzymol.* 546:139–160. https://doi.org/10.1016/B978-0-12-801185-0.00007-6

Dannhauser, P.N., and E.J. Ungewickell. 2012. Reconstitution of clathrin-coated bud and vesicle formation with minimal components. *Nat. Cell Biol.* 14:634–639. https://doi.org/10.1038/ncb2478

Dannhauser, P.N., M. Platen, H. Böning, H. Ungewickell, I.A.T. Schaap, and E.J. Ungewickell. 2015. Effect of clathrin light chains on the stiffness of clathrin lattices and membrane budding. *Traffic.* 16:519–533. https://doi.org/10.1111/tra.12263

Doyon, J.B., B. Zeitler, J. Cheng, A.T. Cheng, J.M. Cherone, Y. Santiago, A.H. Lee, T.D. Vo, Y. Doyon, J.C. Miller, et al. 2011. Rapid and efficient clathrin-mediated endocytosis revealed in genome-edited mammalian cells. *Nat. Cell Biol.* 13:331–337. https://doi.org/10.1038/ncb2175

Drubin, D.G., and A.A. Hyman. 2017. Stem cells: the new "model organism". *Mol. Biol. Cell.* 28:1409–1411. https://doi.org/10.1091/mbc.e17-03-0183

Engler, A.J., S. Sen, H.L. Sweeney, and D.E. Discher. 2006. Matrix elasticity directs stem cell lineage specification. *Cell.* 126:677–689. https://doi.org/10.1016/j.cell.2006.06.044

Ezratty, E.J., C. Bertaux, E.E. Marcantonio, and G.G. Gundersen. 2009. Clathrin mediates integrin endocytosis for focal adhesion disassembly in migrating cells. *J. Cell Biol.* 187:733–747. https://doi.org/10.1083/jcb.200904054

Fortian, A., L.K. Dionne, S.H. Hong, W. Kim, S.P. Gygi, S.C. Watkins, and A. Sorkin. 2015. Endocytosis of Ubiquitylation-Deficient EGFR Mutants via Clathrin-Coated Pits is Mediated by Ubiquitylation. *Traffic.* 16:1137–1154. https://doi.org/10.1111/tra.12314

Fujimoto, L.M., R. Roth, J.E. Heuser, and S.L. Schmid. 2000. Actin assembly plays a variable, but not obligatory role in receptor-mediated endocytosis in mammalian cells. *Traffic.* 1:161–171. https://doi.org/10.1034/j.1600-0854.2000.010208.x

Gharbi, S.I., M.J. Zvelebil, S.J. Shuttleworth, T. Hancox, N. Saghir, J.F. Timms, and M.D. Waterfield. 2007. Exploring the specificity of the PI3K family inhibitor LY294002. *Biochem. J.* 404:15–21. https://doi.org/10.1042/BJ20061489

Gifford, C.A., M.J. Ziller, H. Gu, C. Trapnell, J. Donaghey, A. Tsankov, A.K. Shalek, D.R. Kelley, A.A. Shishkin, R. Issner, et al. 2013. Transcriptional

and epigenetic dynamics during specification of human embryonic stem cells. *Cell.* 153:1149–1163. https://doi.org/10.1016/j.cell.2013.04.037

Grassart, A., A.T. Cheng, S.H. Hong, F. Zhang, N. Zenzer, Y. Feng, D.M. Briner, G.D. Davis, D. Malkov, and D.G. Drubin. 2014. Actin and dynamin2 dynamics and interplay during clathrin-mediated endocytosis. *J. Cell Biol.* 205:721–735. https://doi.org/10.1083/jcb.201403041

Grove, J., D.J. Metcalf, A.E. Knight, S.T. Wavre-Shapton, T. Sun, E.D. Protonotarios, L.D. Griffin, J. Lippincott-Schwartz, and M. Marsh. 2014. Flat clathrin lattices: stable features of the plasma membrane. *Mol. Biol. Cell.* 25:3581–3594. https://doi.org/10.1091/mbc.e14-06-1154

Heuser, J. 1980. Three-dimensional visualization of coated vesicle formation in fibroblasts. *J. Cell Biol.* 84:560–583. https://doi.org/10.1083/jcb.84.3.560

Hockemeyer, D., H. Wang, S. Kiani, C.S. Lai, Q. Gao, J.P. Cassady, G.J. Cost, L. Zhang, Y. Santiago, J.C. Miller, et al. 2011. Genetic engineering of human pluripotent cells using TALE nucleases. *Nat. Biotechnol.* 29:731–734. https://doi.org/10.1038/nbt.1927

Hoffman, L.M., C.C. Jensen, S. Kloeker, C.L.A. Wang, M. Yoshigi, and M.C. Beckerle. 2006. Genetic ablation of zyxin causes Mena/VASP mislocalization, increased motility, and deficits in actin remodeling. *J. Cell Biol.* 172:771–782. https://doi.org/10.1083/jcb.200512115

Hong, S.H., C.L. Cortesio, and D.G. Drubin. 2015. Machine-Learning-Based Analysis in Genome-Edited Cells Reveals the Efficiency of Clathrin-Mediated Endocytosis. Cell Rep. 12:2121–2130. doi:. https://doi.org/10.1016/j.celrep.2015.08.048

Kadlecova, Z., S.J. Spielman, D. Loerke, A. Mohanakrishnan, D.K. Reed, and S.L. Schmid. 2017. Regulation of clathrin-mediated endocytosis by hierarchical allosteric activation of AP2. *J. Cell Biol.* 216:167–179. https://doi.org/10.1083/jcb.201608071

Kreitzer, F.R., N. Salomonis, A. Sheehan, M. Huang, J.S. Park, M.J. Spindler, P. Lizarraga, W.A. Weiss, P.-L. So, and B.R. Conklin. 2013. A robust method to derive functional neural crest cells from human pluripotent stem cells. *Am. J. Stem Cells.* 2:119–131.

Lampe, M., F. Pierre, S. Al-Sabah, C. Krasel, and C.J. Merrifield. 2014. Dual single-scission event analysis of constitutive transferrin receptor (TfR) endocytosis and ligand-triggered β2-adrenergic receptor (β2AR) or Mu-opioid receptor (MOR) endocytosis. *Mol. Biol. Cell.* 25:3070–3080. https://doi.org/10.1091/mbc.e14-06-1112

Lampe, M., S. Vassilopoulos, and C. Merrifield. 2016. Clathrin coated pits, plaques and adhesion. *J. Struct. Biol.* 196:48–56. https://doi.org/10.1016/j.jsb.2016.07.009

Leyton-Puig, D., T. Isogai, E. Argenzio, B. van den Broek, J. Klarenbeek, H. Janssen, K. Jalink, and M. Innocenti. 2017. Flat clathrin lattices are dynamic actin-controlled hubs for clathrin-mediated endocytosis and signalling of specific receptors. *Nat. Commun.* 8:16068. https://doi.org/10.1038/ncomms16068

Liberali, P., B. Snijder, and L. Pelkmans. 2014. A hierarchical map of regulatory genetic interactions in membrane trafficking. *Cell.* 157:1473–1487. https://doi.org/10.1016/j.cell.2014.04.029

McMahon, H.T., and E. Boucrot. 2011. Molecular mechanism and physiological functions of clathrin-mediated endocytosis. *Nat. Rev. Mol. Cell Biol.* 12:517–533. https://doi.org/10.1038/nrm3151

Miller, S.E., S. Mathiasen, N.A. Bright, F. Pierre, B.T. Kelly, N. Kladt, A. Schauss, C.J. Merrifield, D. Stamou, S. Höning, and D.J. Owen. 2015. CALM regulates clathrin-coated vesicle size and maturation by directly sensing and driving membrane curvature. *Dev. Cell.* 33:163–175. https://doi.org/10.1016/j.devcel.2015.03.002

Posor, Y., M. Eichhorn-Gruenig, D. Puchkov, J. Schöneberg, A. Ullrich, A. Lampe, R. Müller, S. Zarbakhsh, F. Gulluni, E. Hirsch, et al. 2013. Spatiotemporal control of endocytosis by phosphatidylinositol-3,4-bisphosphate. *Nature.* 499:233–237. https://doi.org/10.1038/nature12360

Ran, F.A., P.D. Hsu, C.-Y. Lin, J.S. Gootenberg, S. Konermann, A.E. Trevino, D.A. Scott, A. Inoue, S. Matoba, Y. Zhang, and F. Zhang. 2013. Double nicking by RNA-guided CRISPR Cas9 for enhanced genome editing specificity. *Cell.* 154:1380–1389. https://doi.org/10.1016/j.cell.2013.08.021

Reis, C.R., P.-H. Chen, S. Srinivasan, F. Aguet, M. Mettlen, and S.L. Schmid. 2015. Crosstalk between Akt/GSK3β signaling and dynamin-1 regulates clathrin-mediated endocytosis. *EMBO J.* 34:2132–2146. https://doi.org/10.15252/embj.201591518

Robinson, M.S. 2015. Forty Years of Clathrin-coated Vesicles. *Traffic.* 16:1210–1238. https://doi.org/10.1111/tra.12335

Rosendale, M., D. Jullié, D. Choquet, and D. Perrais. 2017. Spatial and Temporal Regulation of Receptor Endocytosis in Neuronal Dendrites Revealed by Imaging of Single Vesicle Formation. *Cell Rep.* 18:1840–1847. https://doi.org/10.1016/j.celrep.2017.01.081

Saffarian, S., E. Cocucci, and T. Kirchhausen. 2009. Distinct dynamics of endocytic clathrin-coated pits and coated plaques. *PLoS Biol.* 7:e1000191. https://doi.org/10.1371/journal.pbio.1000191

Scott, B.L., K.A. Sochacki, S.T. Low-Nam, E.M. Bailey, Q. Luu, A. Hor, A.M. Dickey, S. Smith, J.G. Kerkvliet, J.W. Taraska, and A.D. Hoppe. 2018. Membrane bending occurs at all stages of clathrin-coat assembly and defines endocytic dynamics. *Nat. Commun.* 9:419. https://doi.org/10.1038/s41467-018-02818-8

Sochacki, K.A., A.M. Dickey, M.-P. Strub, and J.W. Taraska. 2017. Endocytic proteins are partitioned at the edge of the clathrin lattice in mammalian cells. *Nat. Cell Biol.* 19:352–361. https://doi.org/10.1038/ncb3498

Soldner, F., D. Hockemeyer, C. Beard, Q. Gao, G.W. Bell, E.G. Cook, G. Hargus, A. Blak, O. Cooper, M. Mitalipova, et al. 2009. Parkinson's disease patient-derived induced pluripotent stem cells free of viral reprogramming factors. *Cell.* 136:964–977. https://doi.org/10.1016/j.cell.2009.02.013

Sorkin, A., and M. von Zastrow. 2009. Endocytosis and signalling: intertwining molecular networks. *Nat. Rev. Mol. Cell Biol.* 10:609–622. https://doi.org/10.1038/nrm2748

Taylor, M.J., D. Perrais, and C.J. Merrifield. 2011. A high precision survey of the molecular dynamics of mammalian clathrin-mediated endocytosis. *PLoS Biol.* 9:e1000604. https://doi.org/10.1371/journal.pbio.1000604

Taylor, M.J., M. Lampe, and C.J. Merrifield. 2012. A feedback loop between dynamin and actin recruitment during clathrin-mediated endocytosis. *PLoS Biol.* 10:e1001302. https://doi.org/10.1371/journal.pbio.1001302

Yarar, D., C.M. Waterman-Storer, and S.L. Schmid. 2005. A dynamic actin cytoskeleton functions at multiple stages of clathrin-mediated endocytosis. *Mol. Biol. Cell.* 16:964–975. https://doi.org/10.1091/mbc.e04-09-0774

Zamir, E., M. Katz, Y. Posen, N. Erez, K.M. Yamada, B.Z. Katz, S. Lin, D.C. Lin, A. Bershadsky, Z. Kam, and B. Geiger. 2000. Dynamics and segregation of cell-matrix adhesions in cultured fibroblasts. *Nat. Cell Biol.* 2:191–196. https://doi.org/10.1038/35008607